Eclipse apodization: realization of occulting spots and Lyot masks

Daniel W. Wilson, Paul D. Maker, John T. Trauger, and Tony B. Hull
Jet Propulsion Laboratory
California Institute of Technology
Pasadena, California 91109

ABSTRACT

A key element in the Eclipse coronagraph is the apodized occulting spot. For exo-planet detection in the presence of a sun-like star, the intensity transmittance at the center of the spot is specified to be less than $1x10^{-8}$ (optical density > 8). It must also taper smoothly with a desired functional form to avoid diffraction artifacts in the angular region of planet detection. From a fabrication point of view, these requirements are very challenging. A candidate technology for fabricating such spots is electron-beam exposure of high-energy beam sensitive (HEBS) glass (a product of Canyon Materials, San Diego, CA). In this work, we have calibrated HEBS glass optical density as a function of electron-beam exposure and attained optical densities up to 7.66 without saturation. We then fabricated occulting spots having various functional forms including circular Gaussian, one-dimensional $sinc^2$, and circular $sinc^2$. Preliminary quantitative analysis of the circular $sinc^2$ occulting spot is encouraging.

Keywords: Occulting spots, coronagraphs, high-energy beam sensitive glass, electron-beam lithography

1. INTRODUCTION

The goal of the Eclipse mission is to perform direct imaging of exo-planets and circumstellar material around nearby stars.[1] This will be accomplished by a coronagraphic telescope[2] that employs active wavefront control[3-5] to produce extremely high quality stellar images. When combined with an *apodized* occulting spot and matched Lyot stop, the angular region around the star will be dark enough to enable direct imaging of jovian planets.[6] The focus of the investigation described here is the fabrication of the apodized occulting spot. For exo-planet detection in the presence of a sun-like star, the intensity transmittance, T, at the center of the spot must be less than $1x10^{-8}$ (optical density, OD > 8), and it must taper smoothly with a desired functional form to avoid diffraction artifacts in the angular region of planet detection. From a fabrication point of view, these requirements are very challenging. A candidate technology for fabricating such spots is electron-beam exposure of high-energy beam sensitive (HEBS) glass, a product of Canyon Materials, Canyon Materials, San Diego, CA. As stated in the Canyon Materials literature[7,8], HEBS glass is a low expansion zinc-borosilicate glass doped (ion-exchanged) with silver-ion containing complex crystals and photo inhibitors. The silver-ion complex crystals in the sensitive layer (typically 3 μm thick) become gray with electron-beam exposure. HEBS glass has been used over the last decade as a means for performing gray-scale photolithography with specific application to fabrication of analog surface relief diffractive optical elements.[9,10]

To determine if HEBS glass is a good material for the fabrication of apodized occulting spots, several questions are addressed in this investigation. In Section 2, we describe our efforts to determine whether the glass can be made dark enough and the optical density calibrated accurately. In Section 3, we carefully examine the analog-dose capabilities of our electron-beam lithography system to determine if we can accurately expose desired occulting spot functional forms. Finally, in Section 4, we describe the fabrication and preliminary characterization of occulting spots having three functional forms. In Section 5, we summarize and point to future work that needs to be done.

2. ELECTRON-BEAM EXPOSURE AND CALIBRATION OF HEBS GLASS

Before making occulting spots with desired functional forms, accurate calibration of the HEBS glass optical density as a function of electron-beam exposure was required. The exposures were performed at Jet Propulsion Laboratory (JPL) using a JEOL 9300FS electron-beam lithography system capable of either 50 kV or 100 kV accelerating voltage. Over the course of our investigation, we have exposed and calibrated several types of HEBS glass from Canyon Materials

including the standard HEBS glass, HEBS GI85 with 3 μm thick sensitive layer, and specially manufactured HEBS GI85 with ~10 μm thick sensitive layer. The thicker sensitive layer was ordered to attain maximum optical density with 100 kV electron exposures. To match the Eclipse science goal of high-contrast imaging at wavelengths from 550 to 950 nm, we chose the HEBS GI85 glasses for further investigation because they exhibit maximum optical density at wavelengths around 800 nm, as shown in the next section.

2.1. Optical density as a function of wavelength

The optical density as a function of wavelength was calibrated by exposing multiple 3 mm square uniform-dose areas and then measuring their transmittance using a spectrophotometer. The result for 50 kV exposure of standard HEBS GI85 (3 μm thick sensitive layer) is shown in Figure 1. We have not yet performed the same measurement for the 10 μm thick sensitive layer HEBS GI85 at 100 kV, but we expect the curves to be similar in shape but significantly higher in peak optical density for the same dose. Because spectroscopy of exo-planets is a goal of planet finding missions, the limited bandwidth of the HEBS glass optical density will be an issue for coronagraphs using these occulting spots. However, the usable bandwidth may be widened if the peak OD can be increased significantly or the dopants in the glass can be tailored for this application.

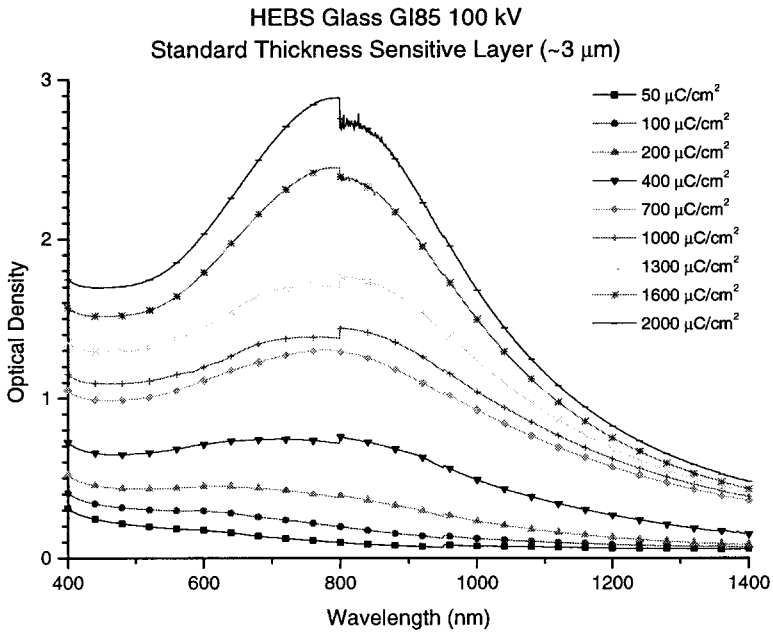

Figure 1. Optical density as a function of wavelength and dose for 50 kV exposure of HEBS GI85 with 3 μm sensitive layer. The steps in the curves at 800 nm are due background subtraction errors after spectrophotometer grating changes.

2.2. Optical density as a function of electron-beam dose

To demonstrate that very high optical densities are attainable, we have performed single-wavelength optical density measurements of 10 μm sensitive layer HEBS GI85 exposed at 100 kV using a diode laser and a picowatt optical power meter as shown in Fig. 2. A stairstep exposure pattern shown in Fig. 3(a) is translated through the beam using a motorized translation stage, and the transmitted power is measured by the optical power meter connected to a computer acting as chart recorder. The measured transmitted power scan data shown in Fig. 3(b) is then averaged across each step and divided by the power through the unexposed glass to yield the transmittance and optical density. The resulting optical density of the 10 μm thick HEBS GI85 exposed at 100 kV is shown in Fig. 4. At a dose of 2553 $\mu C/cm^2$, the measured optical density was 7.66. This value may underestimate the actual OD due to light leakage in the experimental setup. At this dose the OD is clearly not saturated, so it is expected that OD > 8 will be easily attainable.

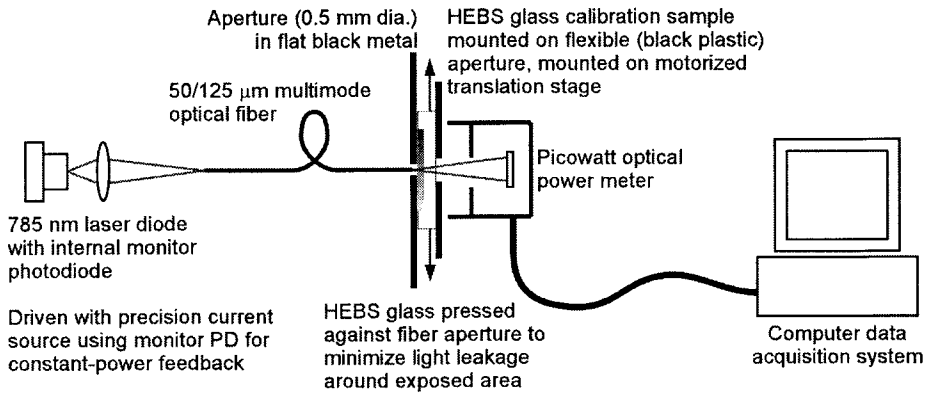

Figure 2. Experimental setup for measuring the optical density of electron-beam exposed HEBS glass

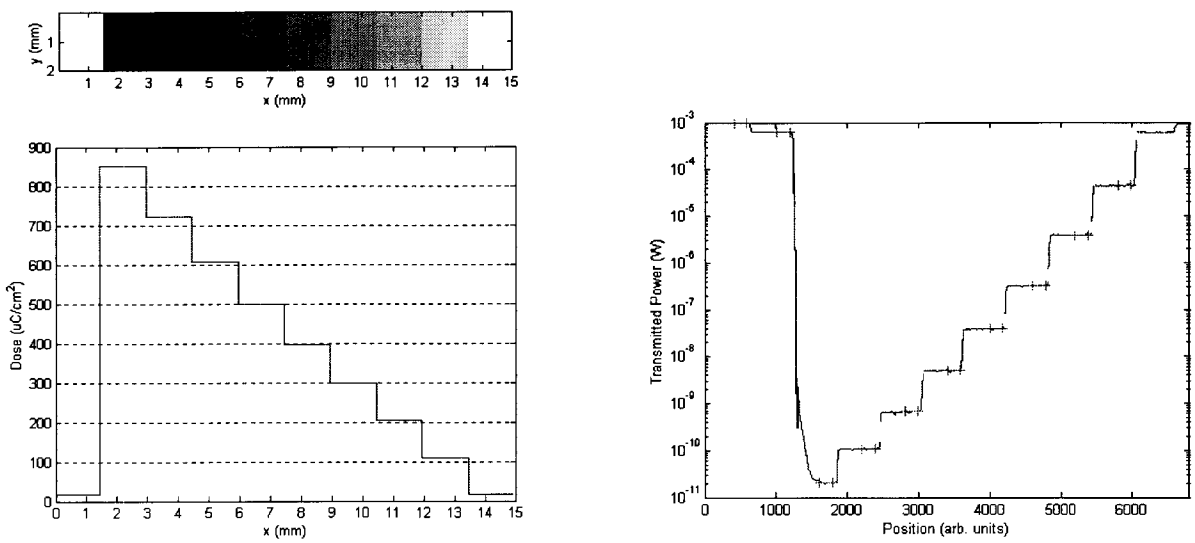

(a) (b)

Figure 3. (a) Example gray-scale E-beam exposure dose pattern for optical density calibration, (b) measured transmitted power using the experimental setup shown in Fig. 2. The crosses indicate regions used for averaging.

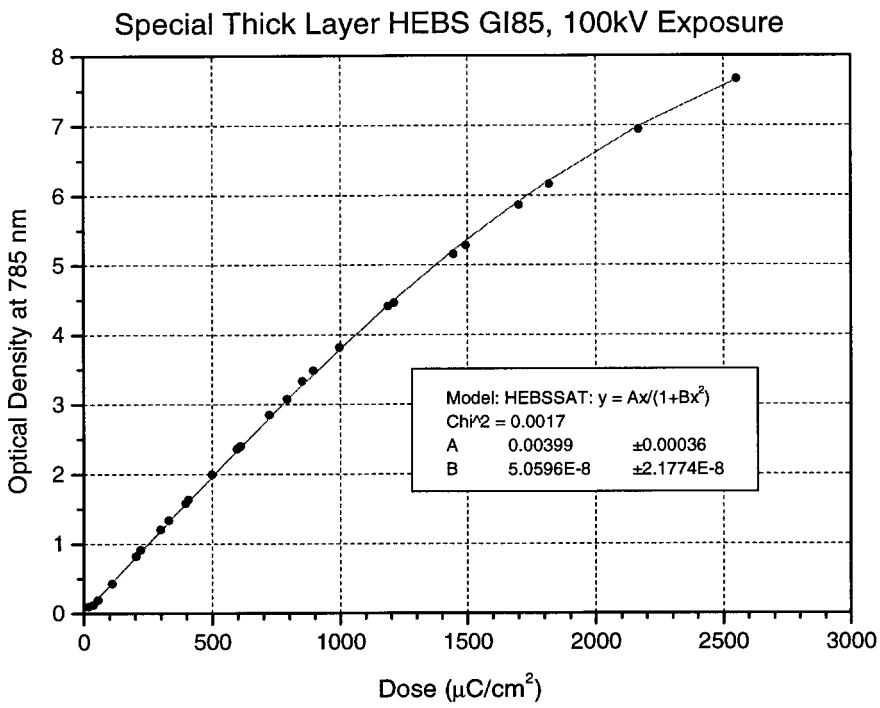

Figure 4. Optical density of thick sensitive layer HEBS GI85 glass at 785 nm as a function of electron-beam dose. The data was fit with the ad hoc saturating function $y = Ax/(1+Bx^2)$ for use in E-beam pattern preparation.

2.3. Electron-beam proximity effect

Our conceptual model of HEBS glass electron-beam exposure has three-dimensional character as shown in Fig. 5(a). The electrons penetrate and darken the HEBS glass sensitive layer and the beam broadens as electrons scatter off atoms in the substrate. This three dimensional scattering (forward and backward) is generally termed the "proximity effect" since it results in exposure around the primary spot. As the electrons undergo multiple scattering events, they lose energy and their ability to expose (darken) the HEBS material changes. An example that clearly illustrates the proximity effect is the alignment cross pattern (10 μm wide bars) shown in Fig. 5(b). The cross was exposed in the HEBS GI85 glass with 10 μm sensitive layer using JPL's JEOL 9300FS electron-beam lithography system operating at 100 kV. The transmission microscope photograph in Fig. 5(b) clearly shows the halo due the proximity effect. Because this photo was taken with broadband illumination, it not suitable for accurate measurement of the proximity effect point spread function strength and radius. We have several experiments planned to characterize the three-dimensional character of the HEBS glass darkening and proximity effect. It should be stressed that the E-beam proximity effect is not an undesirable effect for the occulting spot application since it acts to naturally smooth the spot profile. For accurate occulting spot functional representation, however, the proximity effect point spread function will need to be characterized and deconvolved from the exposure pattern. Over the last decade, we have successfully developed proximity effect characterization and compensation techniques for direct-write E-beam fabrication of analog surface relief profiles in resist,[11-13] and it should be possible to adapt these techniques to the case of gray-scale exposure in HEBS glass.

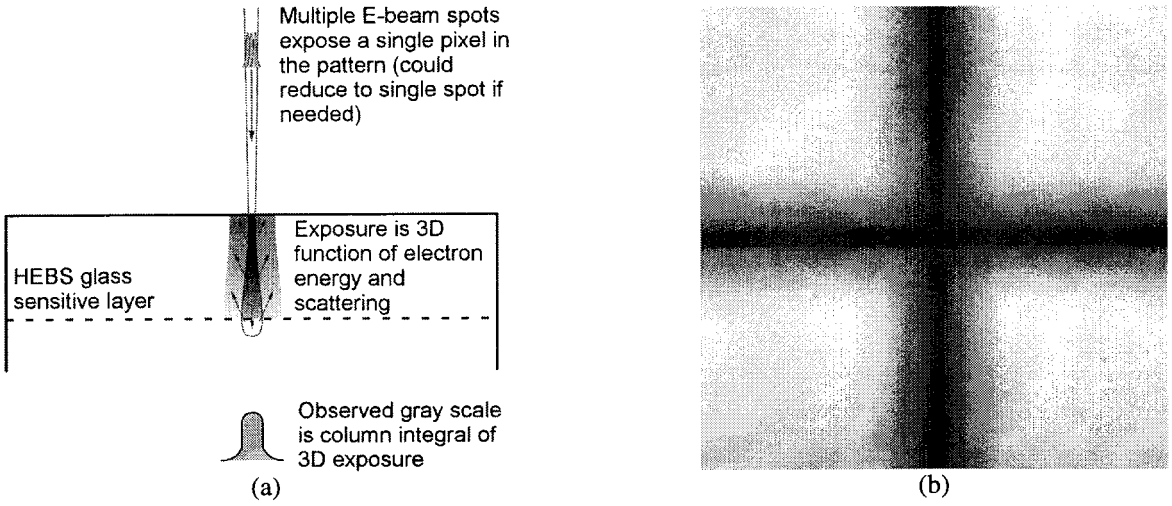

Figure 5. (a) Conceptual model for electron-beam exposure of HEBS glass. (b) Transmission microscope image of alignment cross exposed in thick sensitive layer HEBS GI85 glass at 100 kV. The bars are 10 μm wide and the image was taken using broadband illumination.

3. PATTERN PREPARATION AND EXPOSURE OPTIMIZATION

Using the HEBS glass optical density versus dose calibration curve in Fig. 4, E-beam exposure patterns can be created to realize occulting spots having desired functional forms. During pattern and E-beam job file creation, we try to minimize the errors due to dose quantization that occurs in both software and hardware. Starting from the occulting spot function specification, the flow to an E-beam exposure job file proceeds as follows: (1) the optical density of the spot function is represented as square pixels with sizes less than the wavelength to avoid diffraction effects (typical pixels are 0.1 to 0.5 μm square); (2) the pixel optical densities are converted to E-beam doses ($\mu C/cm^2$) using the measured HEBS glass optical density versus dose calibration curve; (3) the doses are quantized to multiples of 0.001 times a 'base dose' in the job file (typical dose resolution of 0.1 $\mu C/cm^2$); (4) the doses are converted to E-beam dwell times with a minimum clock resolution of 0.2 ns in the E-beam hardware. The effect of the dose quantization that occurs in steps (3) and (4) is best illustrated with an example. If we use a "base dose" of 100 $\mu C/cm^2$, the available doses (job file quantized and range limited) are 0.1, 0.2, 0.3...3299.8, 3299.9, 3300 $\mu C/cm^2$. To reduce the quantization error to 1% for the low doses, we choose a background dose (spot function gets added to this dose) of 10 $\mu C/cm^2$. According to Fig. 4, with this range of doses (10 to 3300) we can attain optical densities from 0.04 ($T = 0.912$) to greater than 8 ($T < 1x10^{-8}$). Hence the job file (software) imposed quantization errors range from 0.1/10 = 0.01 for the low doses (maximum transmittance) and 0.1/3300 = $3x10^{-5}$ for the highest dose (minimum transmittance). We now impose the E-beam dwell time clock minimum resolution of 0.2 ns. At the minimum dose of 10 $\mu C/cm^2$, the dwell time is 40 ns, so the quantization error is 0.2/40 = 0.005. At the maximum dose of 3300 $\mu C/cm^2$, the dwell time is 13200 ns, so the quantization error is 0.2/13200 = $1.5x10^{-5}$. The conclusion is that the hardware quantization error is half that of the software quantization error, and that in darkest region of the spot (center) the quantization error is less than $1x10^{-4}$. At the edges, or at zeros in the function, the quantization error will be around 1%. These errors are favorable for coronagraph occulting spots, since we have the highest gray-scale precision where the incident starlight is the brightest.

4. FABRICATED OCCULTING SPOT RESULTS

Using the procedure described in Section 3, we have fabricated several occulting spots and have begun characterizing them. All spots were fabricated in the thick sensitive layer HEBS GI85 glass. They were exposed using JPL's JEOL 9300FS E-beam lithography system operating at 100 kV accelerating voltage, 20 nA current, 330 μm aperture (spot size ~70 nm), and 50 nm spot-to-spot spacing. The pixel size used to represent the occulting spot functions was 0.5 μm.

4.1. Circular Gaussian

One of several functional forms being considered for coronagaph occulting spots is the circular Gaussian:

$$T(r) = T_{\max}\left[1 - e^{-(r/\sigma)^2}\right]^2$$
$$T_{\max} = 0.9,\ \ \sigma = 52.0\ \mu\text{m},\ \ r_{\max} = 4\times 52 = 208\ \mu\text{m} \tag{1}$$

where the radial parameter, σ, was chosen to produce a spot having half-maximum transmittance at a radius equal to $4\lambda/D$ (at λ = 800 nm) for the f/18 Eclipse testbed[14] telescope. The gray-scale intensity and cross section of the spot design in shown in Fig. 6(a) and (b). A broadband-illuminated transmission microscope photo of the fabricated spot is shown Fig. 6(c). Due to the broadband illumination and the quality of the photograph, no quantitative analysis of the image was performed.

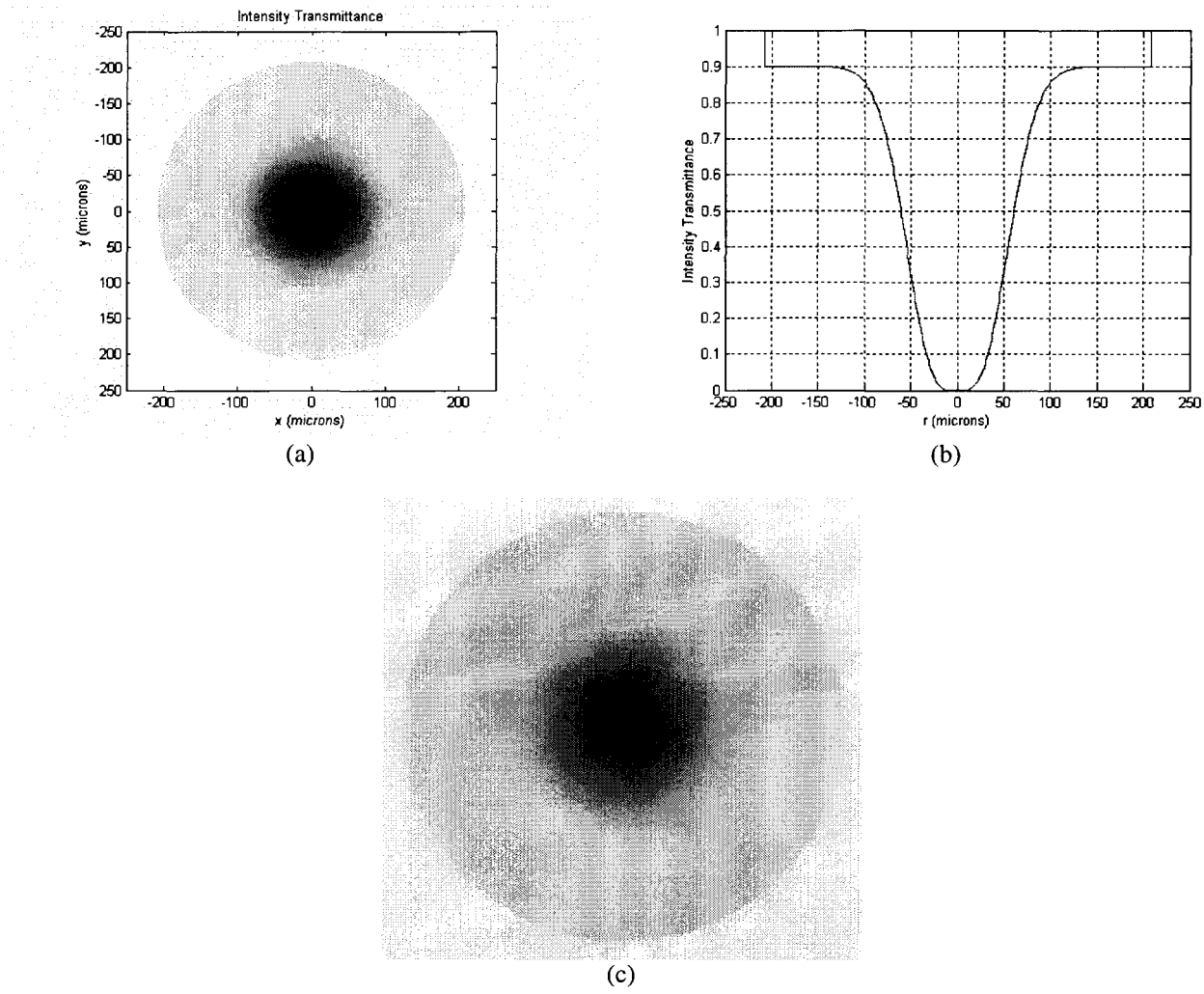

Figure 6. (a) Gray-scale representation of the designed intensity transmittance, (b) cross-section of the design intensity transmittance, (c) transmission microscope image of the E-beam fabricated spot (broadband illumination).

4.2. One-dimensional sinc^2

Another functional form being considered is the one-dimensional sinc^2 spot[15],

$$T(x) = T_{\max}\left[1-\left[\frac{\sin(\pi x/w)}{\pi x/w}\right]^2\right]^2 \tag{2}$$

$$T_{\max} = 0.9,\ w = 82.9\ \mu\text{m},\ x_{\max} = \pm 4\times 82.9 = \pm 331.6\ \mu\text{m}$$

where the width parameter, w, was chosen to produce a spot having half-maximum transmittance at a half-width equal to $4\lambda/D$ (at λ = 800 nm) for the f/18 Eclipse testbed[14] telescope. The gray-scale intensity and cross section of the spot design is shown in Fig. 7(a) and (b). A broadband-illuminated transmission microscope photo of the fabricated spot is shown in Figure 7(c). The quality of the photograph is again not suitable for quantitative analysis, but it clearly shows the desired sinc^2 oscillations.

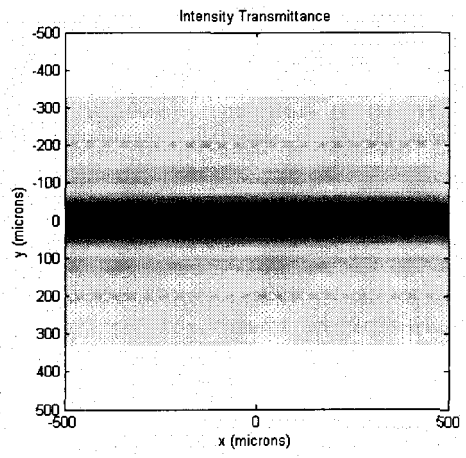

(a)

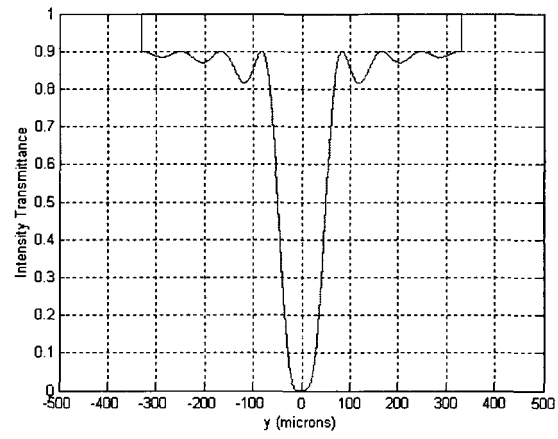

(b)

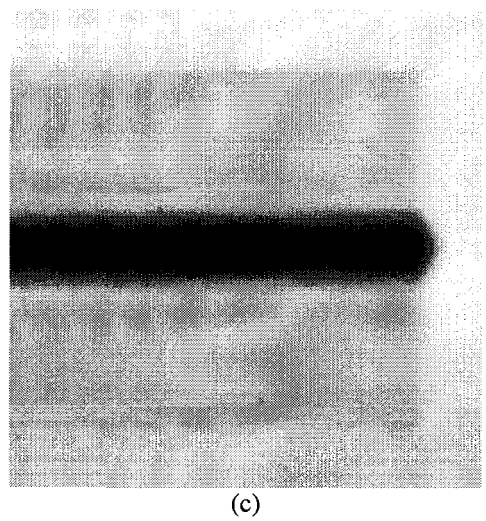

(c)

Figure 7. (a) Gray-scale representation of the designed intensity transmittance, (b) cross-section of the design intensity transmittance, (c) transmission microscope image of the E-beam fabricated spot (broadband illumination).

4.3. Circular sinc^2

A simple generalization of the linear sinc^2 spot to polar coordinates is the circular sinc^2 spot,

$$T(r) = T_{\max}\left[1-\left[\frac{\sin(\pi r/w)}{\pi r/w}\right]^2\right]^2 \tag{3}$$

$$T_{\max} = 0.9,\ \ w = 100.5\ \mu\text{m},\ \ r_{\max} = 4\times 100.5 = 402.0\ \mu\text{m}$$

where again the radial parameter, w, was chosen to produce a spot having half-maximum transmittance at a radius equal to $4\lambda/D$ (at λ = 800 nm) for the f/18 Eclipse testbed[14] telescope. The gray-scale intensity and cross section of the spot design in shown in Fig. 8(a) and (b). A high quality microscope photo of the fabricated spot (800 nm illumination, 16-bit gray-scale, background divided out) is shown Figure 8(c). Figure 8(d) shows the spot using a hard stretched colormap to reveal E-beam lithography dose errors. The center 500 μm square region is an E-beam "field" over which the stage does not move. The spot pattern was intentionally positioned at the center of a 3x3 array of E-beam fields to avoid a field boundary at or near the center of the spot. However, the stretched image clearly shows that the dose varies slightly from field-to-field, with increased dose in fields that have more pixels. This error is relatively small on an absolute scale, but significantly larger than the quantization errors discussed earlier. It is currently being quantified and investigated as to the cause. In the absence of a hardware fix, it may be possible to adjust the dose of each field in software to achieve uniformity.

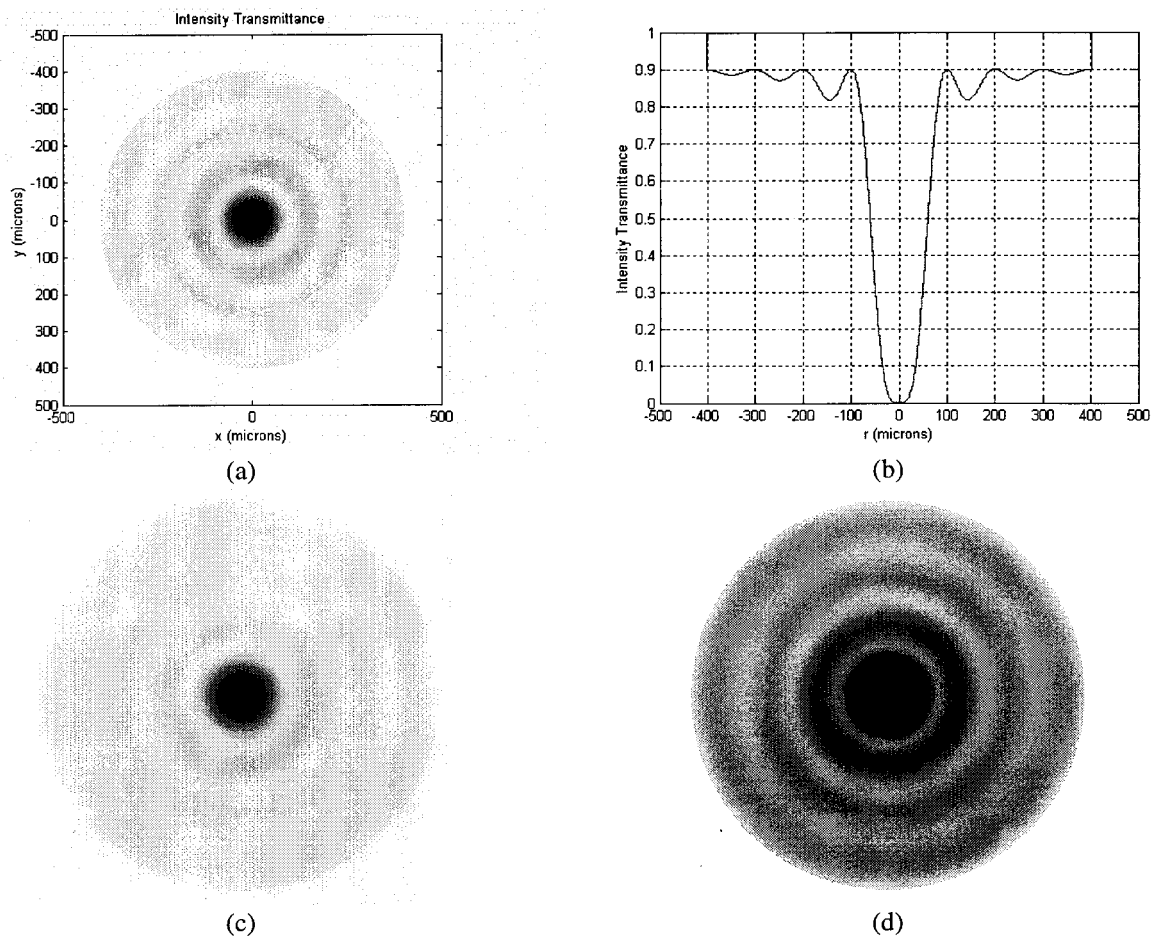

Figure 8. (a) Gray-scale representation of the designed intensity transmittance, (b) cross-section of the design intensity transmittance, (c) transmission microscope image of the E-beam fabricated spot (broadband illumination), (d) same image as in (c) with a hard-stretched colormap to reveal exposure non-uniformity.

The unstretched image in Fig. 8(c) was quantitatively analyzed by finding the center and then averaging 36 radial slices as shown in Fig. 9(a) and (b). The average intensity transmittance as a function of radius is compared to the design in Fig. 9(c). The discrepancies between the measured and designed transmittance are consistent with the E-beam proximity effect and experimental imaging errors. The difference in darkness at the center of the spot is likely due to improper illumination conditions and background subtraction error. The differences in the oscillatory portion of the function can be attributed to convolution of the design pattern with the proximity effect point spread function (PSF). That is, if we assume a Gaussian PSF for the proximity effect, convolution of that PSF with the sinc^2 dose distribution will fill-in the oscillations in the function and decrease their amplitude, just as we observe in Fig. 9(c).

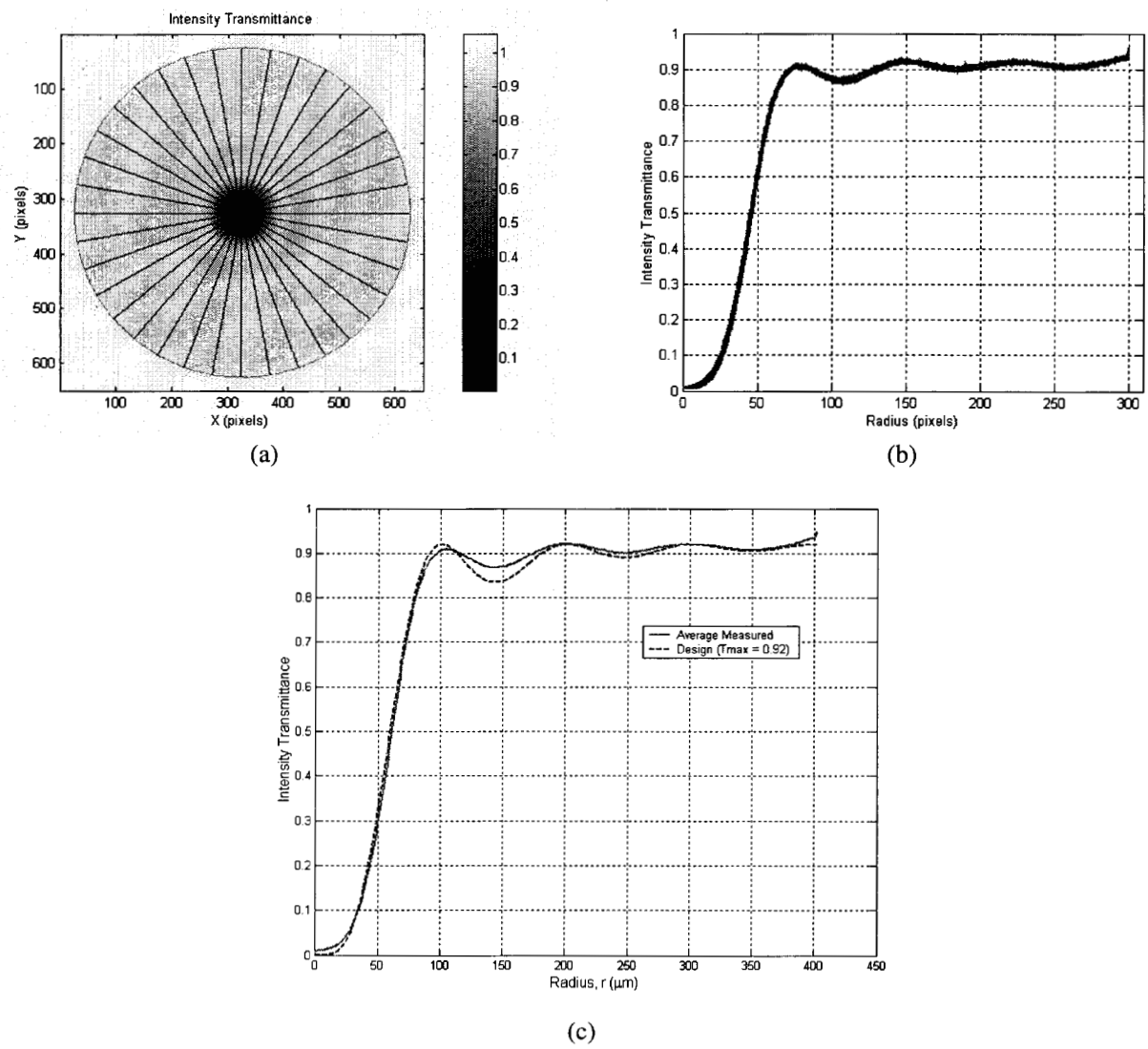

Figure 9. Quantitative analysis of the circular sinc^2 occulting spot: (a) radial slices through intensity transmittance image, (b) all slices plotted together to show noise level, (c) average of radial slices plotted together with the design transmittance curve (slightly scaled) for comparison.

5. SUMMARY AND FUTURE WORK

The results presented here show that electron-beam exposure of HEBS glass is a promising technology for fabrication of apodized occulting spots. The positive attributes are high optical density (OD > 8) and precise control of the gray-scale transmittance to realize nearly arbitrary apodizing functions. The latter capability is made possible by the high level of dose control in state-of-the-art electron-beam lithography tools such as the JEOL 9300FS. To ultimately realize accurate apodizing functional forms, we will need to characterize and compensate for the E-beam proximity effect in HEBS glass. Accurate characterization of apodized high-optical-density occulting spots is difficult because scattering in the optical system (point-by-point or imaging) decreases the measured optical density. The ultimate test for the fabricated occulting spots will be their validation in the Eclipse testbed at JPL.[14] For space-based coronagraphs such as Eclipse, there are two major questions as to the applicability of HEBS glass occulting spots. First, we need to understand its sensitivity to radiation present in a space environment. Second, we need to investigate techniques for increasing the spectral bandwidth over which high optical density is attainable.

ACKNOWLEDGEMENTS

We would like to Chuck Wu at Canyon Materials for helpful discussions and for agreeing to fabricate the custom HEBS glass with extra thick sensitive layer. We would also like to thank Richard Muller at JPL for performing the electron-beam lithography.

REFERENCES

1. J. T. Trauger, "Eclipse mission: a direct survey of nearby planets," Proc. SPIE 4854-38, 2002.
2. T. Hull, J. T. Trauger, S. A. Macenka, D. Moody, G. Olarte, C. Sepulveda, W. Tsuha, D. Cohen, "Eclipse Telescope Design Factors," Proc. SPIE 4860-49, 2002.
3. J. T. Trauger, D. Moody, B. Gordon, Y. Gursel, M. A. Ealey, R. B. Bagwell, "Performance of a precision high-density deformable mirror for extremely high contrast imaging astronomy from space," Proc. SPIE 4854-01, 2002.
4. J. J. Green, D. C. Redding, S. B. Shaklan, "Extreme wavefront sensing accuracy," Proc. SPIE 4860-48, 2002.
5. S. B. Shaklan, J. J. Green, D. Moody, "Residual wavefront phase estimation in the Lyot plane for the eclipse coronagraphic telescope," Proc. SPIE 4860-42, 2002.
6. T. Hull, J. T. Trauger, D. C. Redding, J. J. Green, "Eclipse architecture," Proc. SPIE 4860-09, 2002.
7. http://www.canyonmaterials.com/prop_hebs1.html
8. C. K. Wu, "High-energy beam-sensitive glasses," U.S. patent 5,285,517, February 8, 1994.
9. W. Daschner, P. Long, R. Stein, C. Wu, and S. H. Lee, "Cost-effective mass fabrication of multilevel diffractive optical elements by use of a single optical exposure with a gray-scale mask on high-energy beam-sensitive glass," Appl. Optics **36**, pp. 4675-4680, July 10, 1997.
10. W. Daschner, P. Long, R. Stein, C. Wu, and S. H. Lee, "General aspheric refractive micro-optics fabricated by optical lithography using a high energy beam sensitive glass gray-level mask," J. Vac. Sci. Technol. **14**, pp. 3730-3733, Nov-Dec 1996.
11. P. D. Maker, and R. E. Muller, "Phase holograms in poly methyl methacrylate," J. Vac. Sci. Technol. B **10**, pp. 2516-2519, Nov-Dec 1992.
12. P. D. Maker and R. E. Muller, "Phase holograms in PMMA with proximity effect correction," NASA CP-3227, pp. 207-221, Feb. 1993.
13. P. D. Maker, D. W. Wilson, and R. E. Muller, "Fabrication and performance of optical interconnect analog phase holograms made be E-beam lithography," in Optoelectronic Interconnects and Packaging, R. T. Chen and P. S. Guilfoyle, eds., Proc. SPIE CR62, pp. 415-430, Jan. 1996.
14. J. T. Trauger, T. Hull, D. C. Redding, F. Shi, Y. Gursel, S. Shaklan, D. Moody, B. Gordon, J. J. Green, A. E. Lowman, D. Cohen, S. A. Bassinger, S. A. Macenka, "Eclipse high-contrast imaging testbed," Proc. SPIE 4854-41, 2002.
15. M. J. Kuchner and W. A. Traub, "A coronagraph with a band-limited mask for finding terrestrial planets," ApJ **570**, pp. 900 (2002).